

BEBOP VI. Enabling the detection of circumbinary planets orbiting double-lined binaries with the DOLBY method of radial-velocity extraction

Lalitha Sairam,^{1,2*} Thomas A. Baycroft,² Isabelle Boisse,³ Neda Heidari,⁴ Alexandre Santerne,³ Amaury H.M.J. Triaud,² Gavin A.L. Coleman,⁵ Yasmin T. Davis,² Magali Deleuil,³ Guillaume Hébrard,⁴ David V. Martin,⁶ Pierre F.L. Maxted,⁷ Richard P. Nelson,⁵ Daniel Sebastian,² Owen J. Scutt,² Matthew R. Standing⁸

¹*Institute of Astronomy, University of Cambridge, Madingley road, Cambridge CB3 0HA, UK*

²*School of Physics and Astronomy, University of Birmingham, Edgbaston, Birmingham B15 2TT, UK*

³*Aix Marseille Univ, CNRS, CNES, LAM, Marseille, France*

⁴*Institut d'astrophysique de Paris, UMR 7095 CNRS université pierre et marie curie, 98 bis, boulevard Arago, 75014, Paris*

⁵*Astronomy Unit, Queen Mary University of London, Mile End Road, London E1 4NS, UK*

⁶*Department of Physics and Astronomy, Tufts University, 574 Boston Avenue, Medford, MA 02155*

⁷*Astrophysics Group, Keele University, ST5 5BG, UK*

⁸*European Space Agency (ESA), European Space Astronomy Centre (ESAC), Madrid, Spain*

Accepted XXX. Received YYY; in original form ZZZ

ABSTRACT

Circumbinary planets - planets that orbit both stars in a binary system - offer the opportunity to study planet formation and orbital migration in a different environment compare to single stars. However, despite the fact that > 90% of binary systems in the solar neighbourhood are spectrally resolved double-lined binaries, there has been only one detection of a circumbinary planet orbiting a double-lined binary using the radial velocity method so far. Spectrally disentangling both components of a binary system is hard to do accurately. Weak spectral lines blend with one another in a time-varying way, and inaccuracy in spectral modelling can lead to an inaccurate estimation of the radial-velocity of each component. This inaccuracy adds scatter to the measurements that can hide the weak radial-velocity signature of circumbinary exoplanets. We have obtained new high signal-to-noise and high-resolution spectra with the SOPHIE spectrograph, mounted on the 193cm telescope at Observatoire de Haute-Provence (OHP) for six, bright, double-lined binaries for which a circumbinary exoplanet detection has been attempted in the past. To extract radial-velocities we use the DOLBY code, a recent method of spectral disentangling using Gaussian processes to model the time-varying components. We analyse the resulting radial-velocities with a diffusive nested sampler to seek planets, and compute sensitivity limits.

We do not detect any new circumbinary planet. However, we show that the combination of new data, new radial-velocity extraction methods, and new statistical methods to determine a dataset's sensitivity to planets leads to an approximately one order of magnitude improvement compared to previous results. This improvement brings us into the range of known circumbinary exoplanets and paves the way for new campaigns of observations targeting double-lined binaries.

Key words: techniques: radial velocities – binaries: spectroscopic – binaries: eclipsing – planets and satellites: detection

1 INTRODUCTION

One of the most remarkable discoveries from the *Kepler* mission is the identification of the first confirmed circumbinary planet, Kepler-16 b (Doyle et al. 2011). This planet orbits both stars of its binary host providing a novel environment to investigate the outcome of planet formation. The discovery of Kepler-16 b was surprising because theoretical work implies that circumbinary configurations prevent the formation of planets at such proximity to the binary (e.g. Meschiari

2012; Paardekooper et al. 2012; Lines et al. 2014; Pierens et al. 2020; Martin & Fitzmaurice 2022). In parallel, once planets have formed, disc-driven orbital migration parks the planets near the instability limit (e.g. Dvorak et al. 1989; Holman & Wiegert 1999; Doolin & Blundell 2011; Coleman et al. 2023a,b) in ways that encodes the conditions of their protoplanetary disc into their observable orbital properties (e.g. Penzlin et al. 2021). Thus, circumbinary planets offer new insights into planet formation mechanisms that will inform planet formation around single stars and that enhance our understanding of the exoplanet population at large, completing the tale behind the origins of the Solar System, and of our Earth.

* E-mail: ls2071@cam.ac.uk

Few circumbinary planets have been discovered so far, and most of them were found by analysing months-long space-based photometric time-series. This is expensive, and inefficient. A ground-based radial velocity survey of binaries is expected to be less biased towards planetary orbital plane perpendicular to the sky than the transit method, while finding as many planets in only a fraction of the telescope time, measuring more orbital parameters, and constructing a leaner, more intuitive picture of the circumbinary population. At the moment, single-lined binaries (SB1) are the only binaries for which a $1\text{--}2\text{ m s}^{-1}$ radial velocity accuracy has been demonstrated (Standing et al. 2022; Triaud et al. 2022), thus allowing for a more reliable planet detection success rate. The BEBOP survey (Binary Escorted by Orbiting Planets; Martin et al. 2019) has monitored a sample of single-lined binary systems in search of circumbinary planets leading to planet detections (e.g. TOI 1338c/ BEBOP-1c; Standing et al. 2023). Several other candidates have also been announced (Baycroft et al. in press). However, in order to truly understand circumbinary systems and their formation, we need to expand the type of binaries around which circumbinary planets can be detected.

Around 90% of binary systems in the solar-neighbourhood are spectrally resolved as double-lined binaries (SB2; Kovaleva et al. 2016), possibly making them the most common circumbinary planet-hosts. This is an opportunity to dramatically increase the sample available for circumbinary planet surveys, and perform better comparisons between the properties of exoplanets orbiting single stars, and the properties of circumbinary planets. Double-lined binaries are on average brighter, further helping with the detection of small-mass exoplanets orbiting them. Furthermore, for each spectrum, two radial velocity measurements are obtained (for each of the components). Additionally, the vast majority of NASA's *TESS* mission (Ricker et al. 2014) might produce serendipitous circumbinary planet candidates as a "*1–2 punch*" transit event on double-lined binaries (Kostov et al. 2020). For most of the sky, only 27-day timeseries are available in *TESS*, and are themselves obtained once typically every other year. Because of circumbinary planet's intrinsically long orbital periods, this implies two transits of a circumbinary planet transits roughly one orbital period away from one another are challenging to obtain (except in *TESS*'s continuous viewing zone as in Kostov et al. 2021). However, within those short sectors, a circumbinary planet can still be identified when it first transits one star, and soon after transits the other star of the binary system, a "*1–2 punch*". For both transit events to be detectable, both stars need to be of comparable brightness, hence, they will most likely be double-lined binaries. Without at least a $1\text{--}2\text{ m s}^{-1}$ accuracy on double-lined binaries, we might never know whether those events are truly produced by planets.

A dedicated search for circumbinary planets using the radial velocity method, TATOOINE, was attempted on ten double-lined binaries (SB2; Konacki et al. 2009, 2010). Despite being the state-of-the-art, their results showed a large scatter of $10\text{--}15\text{ m s}^{-1}$ in radial velocities (sometimes more), although photon noise reaches 1 m s^{-1} in some cases (they also had to deconvolve an iodine reference spectrum). This extra scatter would prevent the detection of most circumbinary gas-giants (assuming similar planet population properties between single and binary stars). This $10\text{--}15\text{ m s}^{-1}$ problem is likely caused by an imperfect disentangling of the time-varying blending of weak spectral lines, as the two components orbit one another, translating across the spectrograph by $\sim 100\text{ km s}^{-1}$. Konacki et al. (2009) disentangled their spectra to achieve a remarkable precision even at current standards, but it was not enough for identifying planets. Many lines have small signal-to-noise on each spectrum and are easy to miss. While individually they appear as noise, when hundreds of those are missed, they likely contribute to a spurious signal. Bi-

nary mask cross-correlation methods also handle line blends badly and those regions are usually avoided. They too produce extra-noise on double-lined binaries, even in 2-dimensional cross-correlations (Zucker et al. 2004).

As part of the BEBOP programme, we invested a small amount of telescope time to observing double-lined binaries, and in creating new ways of extracting radial-velocities for SB2s. In Sairam et al. (2024), we produced two novel methods (now called DOLBY; DOuble-Lined Binary) able to precisely measure the radial velocities of double-lined binaries. DOLBY uses a Gaussian process to help model both spectral components and disentangle them from one another. Applying the DOLBY methods to TIC 172900988, a proposed circumbinary planet transiting a double-lined binary (Kostov et al. 2021), we successfully detected a Doppler variation consistent with a circumbinary planet at an orbital period of $\sim 150\text{ d}$ (Sairam et al. 2024). However, the stars composing the TIC 172900988 system are both fairly hot, for the primary star, we obtained radial-velocity scatters of approximately 40 and 49 m s^{-1} using both the DOLBY-SD and DOLBY-CCF methods, and for the secondary, we obtained scatters of approximately 50 and 72 m s^{-1} , respectively. This scatter did not fully demonstrate the potential of our new approach. In the current paper, we report the DOLBY analysis of our observations of another six SB2 systems that were collected with the SOPHIE spectrograph (Perruchot et al. 2008). All six were specifically taken from the studies by Konacki et al. (2009) and Konacki et al. (2010) to enable a comparison with their results, and test how well the DOLBY methods perform.

This paper is structured as follows: §2 details the observations of SB2 systems used in our analysis. §3 describes the method employed to measure precise radial velocities for the binaries. In §4, we delve into the analysis of the radial velocities, including a comparison between those derived from the traditional TODMOR method. We also discuss the detection limit achieved for the circumbinary method using *kima* for each target system. We conclude the paper with a summary of our key results in §5.

2 A SUMMARY OF OUR DOUBLE-LINED BINARY OBSERVATIONS

In 2019, we initiated a sub-programme targeting 10 double-lined binaries with the SOPHIE spectrograph mounted on the 193cm at Observatoire de Haute-Provence (Perruchot et al. 2008). Our primary objective was to collect a representative sample of double-line binaries, bright and not so bright, across various spectral types and different binary orbital periods with the goal of developing and testing new methods of radial-velocity extraction. Our secondary objective was to detect circumbinary planets in these systems. Our full list includes TIC 172900988, where we first presented the DOLBY methods and detected the circumbinary planet TIC 172900988 b (Sairam et al. 2024). We also survey another three double-lined binaries known to host circumbinary planets, from the *Kepler* field. These are typically faint. The remaining six systems, the subjects of this paper, are HD 195987, HD 210027, HD 9939, HD 78418, HD 13974, and HD 282975 (from the TATOOINE survey; Konacki et al. 2009, 2010). Their properties range $3.76 < V_{\text{mag}} < 10$, $F5 < \text{type} < G6$ and $10 < P_{\text{bin}} < 57\text{ d}$. Compared to the median $V_{\text{mag}} \sim 11.5$ from BEBOP's main sample of single-lined eclipsing binaries (Martin et al. 2019), these six systems are much brighter and highlight well our motivation for observing them and improving radial-velocity measurements for SB2s. The fundamental stellar properties of the targets are summarised in Table 1.

Between 2019-10-09 and 2023-05-06 we collected 244 spectra on the six binaries, with exposure times ranging from 200 to 1800s. We obtained a median signal-to-noise ratio, $\text{SNR} \approx 85$ at 5500 \AA . Some of the observations were obtained in adverse weather conditions, since those systems are bright and could serve as back-up targets. Observations are summarised in Table 1, and spectra are publicly available in the SOPHIE archive.

SOPHIE's high-resolution spectra cover a wide wavelength range from 3872 to 6943 \AA divided into 39 spectral orders, with a resolving power of $\lambda/\delta\lambda \approx 75,000$. The SOPHIE spectrograph was specifically designed to achieve long-term stability of $1 - 2 \text{ m s}^{-1}$, enabling the detection of exoplanets. During the observations, we employed the `fpsimult` mode, utilising one fibre to capture starlight and another fibre towards a Fabry-Pérot lamp, to measure the instrument drift. To ensure accurate wavelength calibration, we performed calibration procedures before the start of each night using a thorium-argon lamp and a Fabry-Pérot.

The data reduction process involved the SOPHIE automatic pipeline (Bouchy et al. 2009), which handled the extraction of the spectra and performed the necessary wavelength calibration. As described in Heidari et al. (2024), an additional colour correction was applied to account for instrumental effects. To ensure the accuracy of our spectroscopic data, we also applied a charge transfer inefficiency (CTI) correction to the SOPHIE spectra. The CTI correction¹ was performed using the method described in Bouchy et al. (2009). Subsequently, we cross-correlated the resulting wavelength-calibrated CTI corrected spectra with a numerical binary mask (Baranne et al. 1996; Pepe et al. 2002). This cross-correlation step allowed us to extract the cross-correlation functions (CCFs), which are essential for our subsequent analysis.

3 A SUMMARY OF THE DOLBY METHOD OF RADIAL-VELOCITY EXTRACTION

In Sairam et al. (2024), we developed two data-driven approaches for accurately measuring radial velocities of double-lined binary systems (SB2s), that we now name DOLBY (DOuble-Lined Binary). Both methods make use of Gaussian Processes (GP) to disentangle both stellar components. The first method works in wavelength space, and makes a spectral decomposition (DOLBY-SD), by modelling the observed spectra of a double-lined binary star as a sum of two GPs Doppler-shifted by their respective radial velocities (the quantity of interest). The second method works in velocity space, using the CCF produced by the SOPHIE pipeline (DOLBY-CCF). Here both components are each modelled as the sum of GPs and of a Gaussian function. The DOLBY-CCF approach is well suited for instruments such as HARPS, SOPHIE and ESPRESSO that produce well characterised and stable CCFs.

In DOLBY-SD, we divide the observed spectra into smaller wavelength subsets or "chunks" and applied GP regression separately to each chunk. This approach allows to account for different spectral types and optimises the reconstruction of the observed spectrum. The method uses a Matérn kernel to model the covariance between the pixels. By exploring the posterior distribution of radial velocities of each chunk and the hyperparameters of the GP functions using a Markov Chain Monte Carlo sampler (MCMC), DOLBY-SD computes refined estimates of the radial velocities for each component.

In DOLBY-CCF, we instead employ a baseline mean function consisting of two Gaussian functions to capture each of the primary and secondary components of the double-lined binary star. In this method, the GPs are used to model the correlated wiggle signal of the CCF for each component using a Matérn covariance kernel. The GP models are optimised using L-BFGS-B method (Byrd et al. 1995) and the posterior distribution of hyperparameters are explored using MCMC sampling in the same way as is done for DOLBY-SD.

Both these methods are effective in accurately measuring the radial velocities of double-lined binary systems. For more details on these methods and their implementation can be found in Sairam et al. (2024). For this paper we chose to use primarily the DOLBY-CCF method, which is by far the easiest to implement and more computationally efficient. This makes it the most likely to be used by other researchers. In the appendix, we provide Tables D1 through D6, which contain the radial velocities obtained using DOLBY-CCF method for the primary and secondary components of each of our targets.

4 RESULTS FROM FITTING THE RADIAL-VELOCITIES

The radial velocities produced by DOLBY-CCF are fit using the *BINARIES* model of `kima` (Faria et al. 2018; Baycroft et al. 2023). `kima` is an orbital fitting algorithm utilising the diffusive nested sampler DNEST4 (Brewer & Foreman-Mackey 2018). `kima` allows the number of Keplerian signals (N_p) applied to the data to be a free parameter. As such we can perform model comparison by computing a Bayes' factor (BF) comparing a system with $N_p = 0$ (a simple binary system) to $N_p = 1$ (or higher numbers of planets too) while keeping all binary and planetary orbital parameters free. `kima` fits for a systemic velocity, and also a radial-velocity jitter term which is added in quadrature to the uncertainties measured from DOLBY-CCF, and is used to account for scatter produced by any unmodelled effects such as stellar variability. The *BINARIES* model takes a different prior for the binary parameters as the planetary ones, using `kima`'s known-object mode. Apsidal precession of the binary orbit is included as an additional free parameter, and a correction to the radial-velocities accounting for relativistic effects² is included (Baycroft et al. 2023). The *BINARIES* model fits SB1 and SB2 radial velocity data equally. In the SB2 case (used in this work), `kima` adjusts models to both the primary and secondary radial velocity time-series simultaneously. A separate systemic velocity and jitter are modelled for each of the primary star and secondary star. We use a Student's *t* distribution in the likelihood evaluation to account for any outliers in the radial velocities. In Fig. A1 and A2, we present the radial velocity time-series for each target, along with the best-fitting binary Keplerian models.

After analysing all six double-lined binaries, we do not detect any planets that pass our detection threshold, $\text{BF} \geq 150$ for a 1-planet model over a 0-planet model (Trotta 2008). We thus consider only the posterior samples where no planet is included to derive the orbital parameters of each of the binaries. We report the fit parameters and Bayes' factors in Table 1. A final advantage of a nested sampler is that it can be used to compute accurate sensitivity limits. We describe that procedure in section §4.7.

Being conscious that nested samplers remain a fairly recent occurrence in the exoplanet scientific literature, we also produce a more classical test. We compute a series of generalised Lomb-Scargle (GLS) periodograms (Zechmeister & Kürster 2009). One

¹ For HD9939 and HD195987 the CTI correction appears to induce a large residual scatter in the data for the secondary star, so for these two cases we do not apply the correction

² These being the light-travel time, transverse doppler, and gravitational redshift effects (Zucker & Alexander 2007; Sybilski et al. 2013)

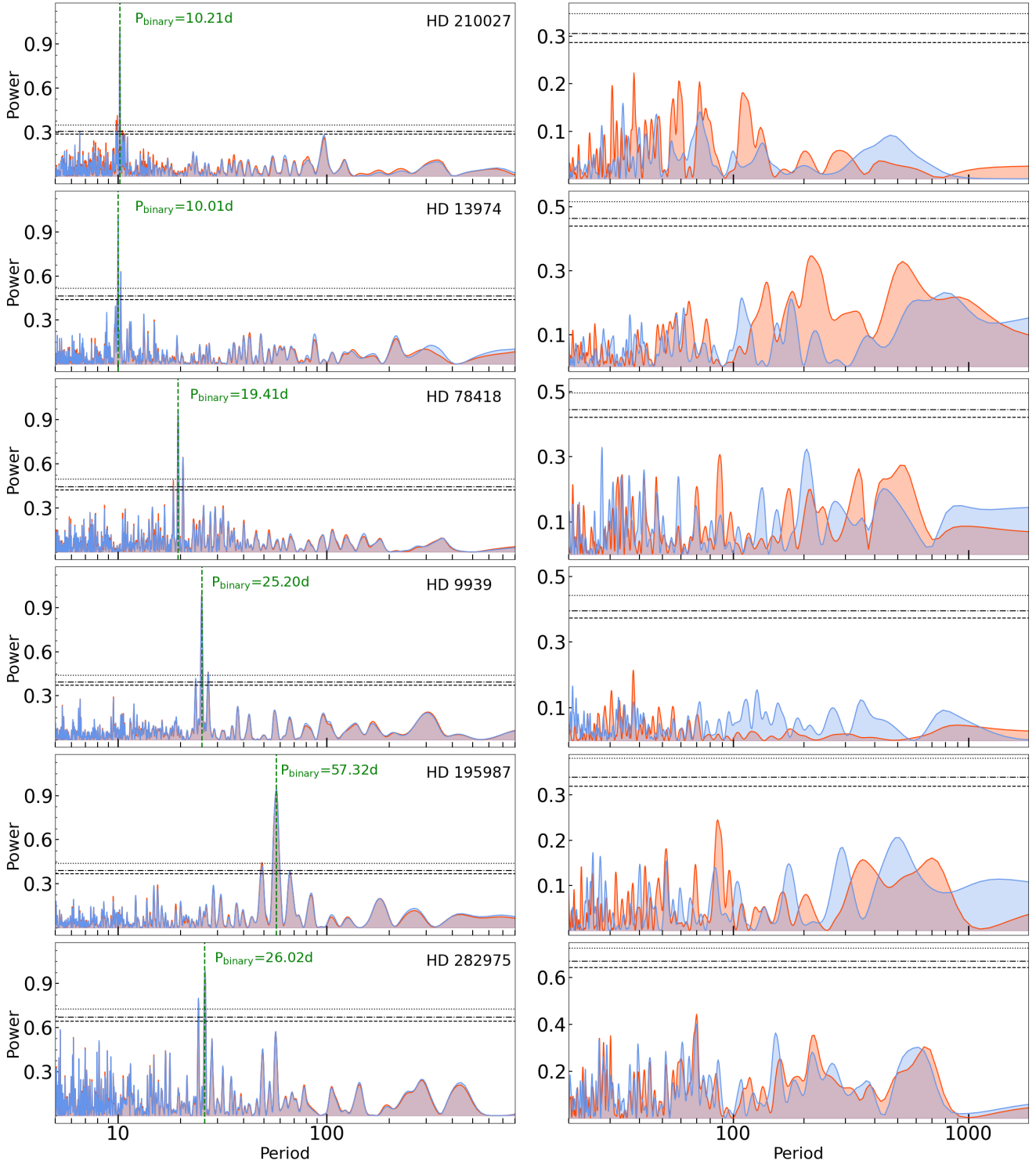


Figure 1. Left panels: Periodogram of radial velocities for the primary (red) and the secondary stars (blue) with binary signal. Right panels: Periodograms after removing the binary motion. The three horizontal lines indicate 10% (dashed line), 5% (dotted dash line), and 1% (dotted line) false alarm probabilities.

periodogram is created for the radial velocities measured of each of the primaries, and for each of the secondary stars (see Figure 1 left panels). Any orbiting object should produce a similar signature in both the primary and secondary sets of radial-velocities, whereas parasitic signals such as stellar variability are expected to only show in one of the two components. The primary and the secondary stars are

depicted in red and blue colours, respectively. We use a 10 000 bootstrap randomisation of each input datasets to compute False Alarm Probabilities (FAP) levels of 10%, 5% and 1%. The significant peaks shown in the left hand side columns of periodograms are associated with the binary star.

To test for the presence of circumbinary exoplanets we compute

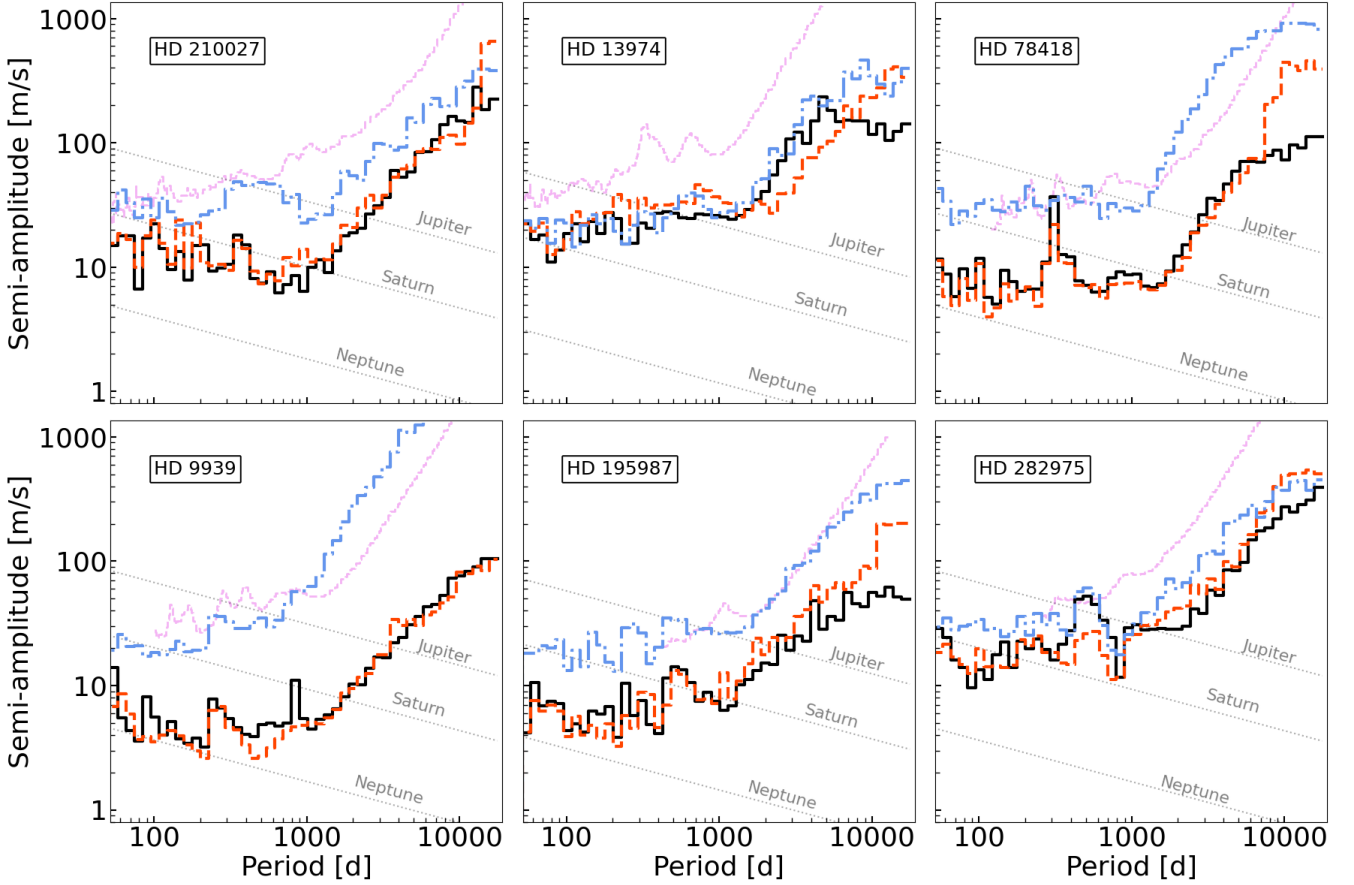


Figure 2. The sensitivity limits based on the density of posterior samples for each binary system from the *kima* run with N_p fixed to 1. Histograms lines show the amplitude at the 99th percentile within each period bin, giving us a 99% confidence upper limit. The red and blue lines represent the analyses using the data solely on the primary and secondary stars respectively, while the black line represents the combined dataset. The violet curves indicate the planet detection limit from Konacki et al. 2009, 2010. Diagonal grey lines are anticipated signals of Neptune, Saturn and Jupiter mass planets orbiting stars with their respective binary masses.

a second series of GLS, after having removed the binary’s orbital motion. To do that we subtract the best fitting Keplerian motion from the *kima* analysis for each of the binary stars (Figure 1 right panels). There are no significant peaks in any of the radial-velocity residuals (right-hand column) that are consistent between the primary and secondary, and also consistent with the results obtained with *kima*.

We now describe the results for every system individually.

4.1 HD 210027

HD 210027 is a bright F5V/G8V spectral type binary system with an orbital period of 10.2 d (Konacki et al. 2010). The SOPHIE observation period spans ~ 800 days. The periodograms for HD 210027 in Fig. 1 (left panel) shows excess at binary period at $P_{\text{bin}} \sim 10.21$ d for both the primary and the secondary star with a FAP value significantly lower than $< 10^{-6}$. Subtracting this signal from the data and recalculating the periodogram (right panel) reveals a few moderate peaks at $5\times$ and $8\times$ the binary period for the primary star’s radial velocities. These peaks have a False Alarm Probability (FAP) of less than 0.05. The Bayes’ Factor for the $N_p = 1$ model vs $N_p = 0$ model is ~ 1.6 . We therefore do not associate this signal with a planetary signal, but possibly with stellar activity on the primary star instead. Our radial velocity solution has rms of 12.5 m s^{-1} and 40.3 m s^{-1} for the pri-

mary and secondary stars, respectively. The $M \sin^3 i$ for the primary and secondary are $1.31174 \pm 0.00031 M_{\odot}$ and $0.81769 \pm 0.00013 M_{\odot}$, with a precision of 0.027% and 0.015%, respectively. Compared to previous work, the mass estimates are $\sim 59\%$ and $\sim 77\%$ more precise for the primary and secondary stars.

4.2 HD 13974

HD 13974 is a 10-d period binary with a spectral type of G0V Konacki et al. (2009). With an observation span extends over ~ 1100 -d, the periodograms for HD 13974 (Fig. 1, left panel) reveal an evident excess at the binary period of approximately $P_{\text{bin}} \sim 10.0177$ days for both the primary and secondary star with FAP $< 10^{-6}$. After removing the strong binary signal from the data, the periodogram is rerun on this binary-subtracted data (shown in the right panel of Fig. 1). This reveals that the primary star’s radial velocity data still exhibits a peak, but the associated FAP is now less than 0.05(5%). The BF for the $N_p = 1$ model vs $N_p = 0$ model is ~ 6.6 . Our radial velocity solution has an rms of 18.1 m s^{-1} for the primary star and 24.9 m s^{-1} for the secondary star.

4.3 HD 78418

HD 78418 is a G5 spectral type binary system with 19.4 d orbital period (Konacki et al. 2010). The periodograms for HD 13974 in Figure 1 (left panel) reveal a notable signal at a binary period of approximately 19.3971 d for both the primary star and with an associated FAP $< 10^{-6}$. When we subtract this signal and re-run the periodogram, as shown in the right panel, we observe a peak at 87.88 d for the primary star and ~ 205 d with FAP < 0.05 (15%) for the secondary star. However, due to the absence of significantly prominent peaks in both stars, we refrain from making definitive comments on the significance of these signals at this stage. The BF for the $N_p = 1$ model vs $N_p = 0$ model is ~ 2.1 . Nevertheless, we intend to continue monitoring this system. The duration of SOPHIE observations spans over 1135 days. The radial velocities derived by our method have an rms of 6.2 and 21 m s^{-1} for the primary and the secondary stars, respectively.

4.4 HD 9939

HD 9939 comprises a binary system characterised by a K0IV spectral type, with an orbital period of 25.2 d (Boden et al. 2006). The SOPHIE observation period spans over 1138 d. The periodograms for HD 9939 in Fig.1 (left panel) shows excess at binary period at ~ 25.2319 d for both the primary and the secondary stars with a FAP $< 10^{-6}$. The radial velocity determined using our methodology, exhibits rms of 5.8 m s^{-1} for the primary star and 63.4 m s^{-1} for the secondary star. We note that the scatter in radial velocity measurements is the largest among all the targets, and we speculate it might be caused by intrinsic variability of this particular star.

The BF for the $N_p = 1$ model vs $N_p = 0$ model is ~ 0.4 . When we subtract the Keplerian signal with a period of ~ 25.2319 days, as depicted in the periodogram (right panel), we observe two peaks at around 38 and 48 days with a FAP exceeding ~ 0.05 (5%) in the radial velocities of the primary star. Stellar variability could potentially be the source of this signal, which warrants further investigation.

4.5 HD 195987

HD 195987 is a G3V/K2V binary system with an orbital period of 57 days (Torres et al. 2002), making it the system with the longest binary period within our set of targets. Our observational coverage with SOPHIE spans ~ 766 days. In the periodogram analysis, a signal emerges at the binary period of ~ 57.3129 d for both the primary and secondary stars with a FAP $< 10^{-6}$. Upon removing this signal from the data, we do not detect any other prominent peaks in the periodogram (Fig. 1, right panel). The BF for the $N_p = 1$ model vs $N_p = 0$ model is ~ 1.2 . In the case of HD 195987, our radial velocity solution produces a rms of 4.8 m s^{-1} for the primary star, effectively reaching the photon noise level, and 27.3 m s^{-1} for the secondary star.

4.6 HD 282975

HD 282975 is a binary system featuring G6V stars with an orbital period of 26 days (Konacki et al. 2009). The duration of our survey extends to 1107 days. The periodogram analysis of the radial velocity data from HD 282975 produces signal at a binary period of ~ 26.1681 days for both the primary and the secondary stars with FAP $< 10^{-6}$. Following the removal of this prominent peak, no other significant peak emerges (Fig. 1, right panel). The BF for the $N_p = 1$ model vs $N_p = 0$ model is ~ 40.6 , a value below the detection threshold of

150. Furthermore, the results of our radial velocity analysis produces an rms of 10.6 m s^{-1} for the primary star and 20.6 m s^{-1} for the secondary star.

4.7 Detection limit

The use of *kima* (and nested sampling in general) lends itself to calculating detection limits in a single analysis. In cases where no planet is detected, as is the case for the systems in this work, we fix the number of Keplerian signals included in the model to one and perform another analysis. The posterior samples resulting from this analysis will then correspond to planetary signals that are consistent with the data but not formally detected. To obtain a detection limit the posterior samples are binned in period with bins of equal width in log-space, then within each bin the detection limit is the value of the semi-amplitude K below which 99% of the posterior samples lie. A more detailed explanation of this method can be found in Standing et al. (2022). To ensure that the detection limit is robust we ensure that each period bin contains at least 1000 posterior samples.

For this work, we perform three detection limits for each binary, the first taking only the radial velocity data for the primary and fitting as a single-lined binary, the second taking only the data for the secondary, and the third taking both and fitting as a double-lined binary. These are shown in Figure 2 alongside the detection limits from Konacki et al. (2009). The diagonal lines indicate the expected signal amplitudes of Neptune, Saturn, and Jupiter mass planets orbiting each binary. We see that our detection limits are consistently more sensitive, up to an order of magnitude better, in the best case. This could come from DOLBY being an improved method at extracting radial-velocities, from an increase in data between Konacki et al. (2010) and our study, and/or from a difference in how the detection limits are estimated.

To further evaluate the performance of our radial-velocity extraction method, we check the influence of data amount and computation of the detection limit. To test the detection limit methods, we first focus on two specific systems, HD 210027 and HD 78418. These systems were chosen because they are the only ones for which we have available radial velocity data from Konacki et al. (2010). We have applied the *kima* method to the radial velocity data from Konacki et al. (2010) for these systems to obtain detection limits. These results are compared with the detection limits derived from our *kima*-DOLBY analysis of the same data and with the original detection limits reported by Konacki et al. (2009). Figure C1 shows the comparison of these detection limits for both systems. The solid black lines represent the detection limits obtained from our *kima*-DOLBY analysis, while the green lines correspond to the detection limits derived from the Konacki data using *kima*. The pink lines indicate the original detection limits reported by Konacki et al. (2009).

In our comparison of detection limits, we consistently observe that DOLBY performs better than previous approaches. Given that we have now employed *kima* on Konacki's radial velocity data and achieved consistent results, the improvement in detection limits is not attributable to the detection limit calculation method itself. Instead, the enhancement could likely be from either the superior accuracy of the DOLBY method or the increased number of measurements.

To quantify the impact of the number of observations, we systematically scaled the Konacki detection limits based on the square root of the relative number of measurements for each system, shown in Figure C2. This scaling assumes that the detection limit improves proportionally with the square root of the number of observations. Our analysis reveals that even after accounting for this scaling, the DOLBY method still demonstrates an improved performance, suggest-

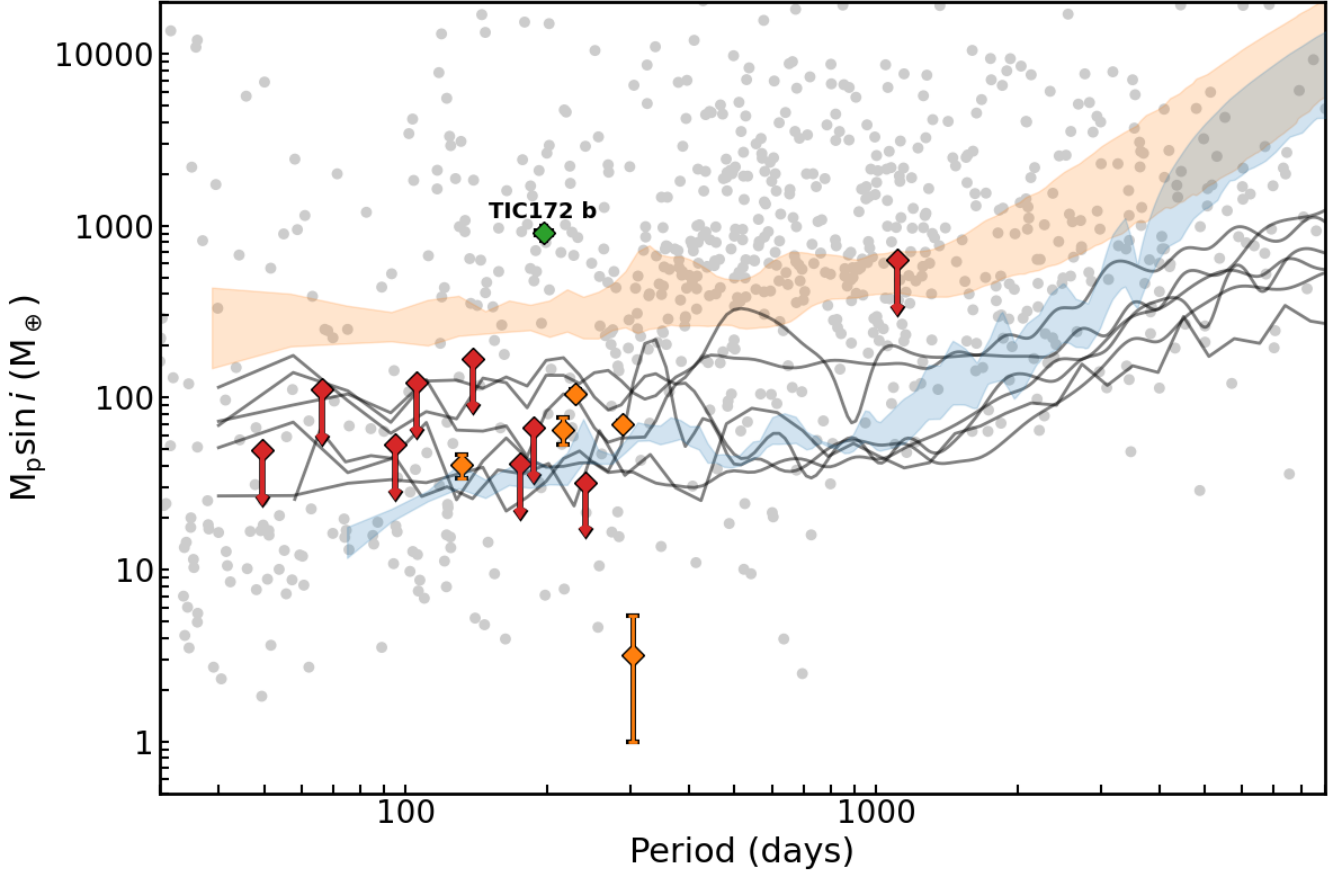


Figure 3. Minimum planet mass versus period plot showcasing the detection limits of DOLBY targets in this study, represented as black lines, alongside confirmed exoplanets as grey circles, and circumbinary planets as orange/red diamonds. Circumbinary planets with upper mass limits are marked with arrows signifying a 2σ upper limit. The blue band denotes the detection limits for SB1 systems (Standing et al. 2022), while the orange band represents the detection limits for SB2 systems (Konacki et al. 2009, 2010). TIC 172900988b is depicted as a green diamond (Sairam et al. 2024).

ing that its inherent accuracy contributes significantly to the observed improvement in detection limits.

4.8 Comparison between methods and datasets

Across the six systems analysed, the mean radial-velocity error for each system ranges between $4.2\text{--}11.6\text{ m s}^{-1}$ for the primaries and $9.3\text{--}44.3\text{ m s}^{-1}$ for the secondaries. In addition, we measure an RMS scatter after removing the most likely binary solution ranging from $4.8\text{--}18.1$ and $20.6\text{--}63.4\text{ m s}^{-1}$ for primaries and secondaries respectively. In all but 3 of the 12 cases the radial velocity jitter that is included in the fit is not constrained and is consistent with 0. This shows that we are reaching a regime where we are photon-noise limited in the best cases. It is also worth noting here that all of the 6 binaries have at least one of the primary and secondary radial velocities close to photon-noise, reinforcing the notion that observing double-lined binaries can be a favourable way to avoid stellar activity relative to single stars or single-lined binaries. When only one component is resolved, and if that component is active, then detecting exoplanets becomes challenging. In the case of double-lined systems, the activity cycle of both stars does not need to be related, and while one star is active, the other star might not be, providing a way to continue the radial-velocity monitoring.

The uncertainties and jitters are shown in Figure B1, where the

box plot showcases the distribution of uncertainties for each binary system and compares them to other results.

We note that DOLBY-CCF systematically outperforms TODMOR (Zucker et al. 2004), the only public code we could directly compare our results to, and analyse the same data with. In addition, the SOPHIE sample analysed with DOLBY produces uncertainties that are systematically smaller than results reported in Konacki et al. (2009, 2010) for the same systems. Also, the DOLBY results typically cover a narrower range of values (i.e. measurements are more consistent with one another). RMS values of the RV residuals are also depicted. Despite using a 2m telescope and collecting on average twice as many measurements for each system, the detection sensitivity obtained with SOPHIE+DOLBY is better in all cases than those reported in Konacki et al. (2009, 2010), even though Konacki et al. used a combination of telescopes including the 10m Keck/Hires, SHANE/CAT/Hamspec, and TNG/SARG. We take this as evidence that the DOLBY method is slightly more accurate than the disentangling method of Konacki et al. (2009, 2010).

5 CONCLUSIONS

This paper presents the application of a novel method, called DOLBY-CCF, to measure radial-velocities of double-lined binary stars with

high precision. We applied DOLBY-CCF to analyse newly collected SOPHIE observations of six double-lined systems previously observed by the TATOOINE survey (Konacki et al. 2009, 2010). Our goal was to assess the capability of DOLBY-CCF for accurate RV measurements of double-lined binary stars, and to assess its potential to detect circumbinary exoplanets.

We achieved a significant improvement in RV precision compared to the traditional TODMOR method (Fig. B1). Our analysis did not reveal any significant detections of circumbinary planets within our sample. Figure 3 depicts a plot of mass versus the orbital period of detection limits obtained from this work for double-lined binaries (black). It also includes detection limits for single-lined binaries (SB1; blue band) obtained by Standing et al. (2022) and confirmed exoplanets (grey filled circles; NASA Exoplanet Archive³). Known transiting circumbinary planets with mass measurements are represented as filled diamonds. We also show the range of detection limits reported by Konacki et al. (2009, 2010) as an orange band. While detection limits for single-lined binaries by Standing et al. (2022) are compatible to the DOLBY-CCF method for SB2s, our analysis offers up to one order-of-magnitude improvement in sensitivity compared to the previous results reported in Konacki et al. (2009, 2010). This improvement could come from various sources: 1) greater accuracy in the radial-velocity extraction, 2) more radial-velocity measurements, and 3) improved methods to compute sensitivity limits, however, by analysing publicly available data from Konacki et al. (2010), and rescaling detection limits to account of differences in the number of measurements, we show that the main improvement is most likely because DOLBY-CCF extracts more accurate radial-velocities than previous methods. Figure 3 also showcases it is now possible to detect circumbinary planets with masses below that of Saturn for orbital periods of up to 1000 days—mirroring the detection capacity observed in single-lined binaries (Standing et al. 2022). The high RV precision achieved by DOLBY-CCF paves the way for future, more sensitive searches for circumbinary planets around double-lined binary stars.

Future work will involve applying DOLBY-CCF to a larger sample of double-lined binary stars and incorporating additional observations to increase the sensitivity of our planet searches. In addition, we aim to test the DOLBY-SD method to compare it to the CCF approach. Our current results however demonstrate that DOLBY represents a valuable, public tool capable of advancing our understanding of circumbinary systems and their potential to harbour exoplanets.

ACKNOWLEDGEMENTS

This paper is based on observations collected at the Observatoire de Haute Provence (OHP). We are grateful to the entire staff at OHP, especially the night assistants, for their dedication and hard work in securing these observations, particularly during the challenging times of the COVID pandemic.

This research was funded by the European Research Council (ERC) under the European Union’s Horizon 2020 research and innovation programme (grant agreement no. 803193/BEBOP) and by the Leverhulme Trust (research project grant no. RPG-2018-418). PM acknowledges support from STFC research grant number ST/S001301/1. MRS acknowledges support from the European Space Agency as an ESA Research Fellow. IB, GH, AS, MD acknowledge the Programme National de Planetologie (PNP) of the CNRS

INSU co-funded by CNES for the funds received to support this work. The acquisition of data was facilitated by a series of allocations through the French PNP. The computations for this research were performed using the University of Birmingham’s BlueBEAR HPC service <http://www.birmingham.ac.uk/bear>.

DATA AVAILABILITY

The full radial velocity data for this study are provided in the appendix. Reduced spectra used in the analysis are publicly available through the SOPHIE archive <http://atlas.obs-hp.fr/sophie/>.

REFERENCES

- Baranne et al., 1996, *Astron. Astrophys. Suppl. Ser.*, 119, 373
 Baycroft T. A., TriAUD A. H. M. J., Faria J., Correia A. C. M., Standing M. R., 2023, *MNRAS*, 521, 1871
 Boden A. F., Torres G., Latham D. W., 2006, *ApJ*, 644, 1193
 Bouchy F., Isambert J., Lovis C., Boisse I., Figueira P., Hébrard G., Pepe F., 2009, in Kern P., ed., *EAS Publications Series Vol. 37*, EAS Publications Series, pp 247–253, doi:10.1051/eas/0937031
 Brewer B. J., Foreman-Mackey D., 2018, *Journal of Statistical Software*, 86, 1
 Byrd R. H., Lu P., Nocedal J., Zhu C., 1995, *SIAM Journal on Scientific Computing*, 16, 1190
 Coleman G. A. L., Nelson R. P., TriAUD A. H. M. J., 2023a, *Monthly Notices of the Royal Astronomical Society*, 522, 4352
 Coleman G. A. L., Nelson R. P., TriAUD A. H. M. J., Standing M. R., 2023b, *Monthly Notices of the Royal Astronomical Society*, 527, 414
 Doolin S., Blundell K. M., 2011, *MNRAS*, 418, 2656
 Doyle L. R., et al., 2011, *Science*, 333, 1602
 Dvorak R., Froeschle C., Froeschle C., 1989, *A&A*, 226, 335
 Faria J. P., Santos N. C., Figueira P., Brewer B. J., 2018, *The Journal of Open Source Software*, 3, 487
 Heidari N., et al., 2024, *Astronomy & Astrophysics*, 681, A55
 Holman M. J., Wiegert P. A., 1999, *AJ*, 117, 621
 Konacki M., Muterspaugh M. W., Kulkarni S. R., Helminiak K. G., 2009, *ApJ*, 704, 513
 Konacki M., Muterspaugh M. W., Kulkarni S. R., Helminiak K. G., 2010, *ApJ*, 719, 1293
 Kostov V. B., et al., 2020, *AJ*, 160, 174
 Kostov V. B., et al., 2021, *AJ*, 162, 234
 Kovaleva D., Malkov O., Yungelson L., Chulkov D., 2016, *Baltic Astronomy*, 25, 419
 Lines S., Leinhardt Z. M., Paardekooper S., Baruteau C., Thebault P., 2014, *ApJ*, 782, L11
 Martin D. V., Fitzmaurice E., 2022, *MNRAS*, 512, 602
 Martin D. V., et al., 2019, *A&A*, 624, A68
 Meschiari S., 2012, *The Astrophysical Journal Letters*, 761, L7
 Paardekooper S.-J., Leinhardt Z. M., Thebault P., Baruteau C., 2012, *The Astrophysical Journal Letters*, 754, L16
 Penzlin A. B. T., Kley W., Nelson R. P., 2021, *A&A*, 645, A68
 Pepe F., Mayor M., Galland F., Naef D., Queloz D., Santos N. C., Udry S., Burnet M., 2002, *A&A*, 388, 632
 Perruchot S., et al., 2008, in McLean I. S., Casali M. M., eds, Vol. 7014, *Ground-based and Airborne Instrumentation for Astronomy II*. SPIE, pp 235 – 246, doi:10.1117/12.787379, <https://doi.org/10.1117/12.787379>
 Pierens A., McNally C. P., Nelson R. P., 2020, *MNRAS*, 496, 2849
 Ricker G. R., et al., 2014, in Oschmann Jacobus M. J., Clampin M., Fazio G. G., MacEwen H. A., eds, *Society of Photo-Optical Instrumentation Engineers (SPIE) Conference Series Vol. 9143*, *Space Telescopes and Instrumentation 2014: Optical, Infrared, and Millimeter Wave*. p. 914320 (arXiv:1406.0151), doi:10.1117/12.2063489
 Sairam L., et al., 2024, *MNRAS*, 527, 2261

³ <https://exoplanetarchive.ipac.caltech.edu/index.html>

Table 1. Properties of SB2s

Parameters	HD 210027	HD 13974	HD 78418	HD 9939	HD 195987	HD 282975
V (mag)	3.76	4.9	5.98	6.99	7.09	10.0
Spectral type	F5V/G8V	G0V	G5	K0IV	G3V/K2V	G6V
Effective temperatures (K)	6642/4991		6000/5900			
Number of epochs	56	35	37	43	52	21
i	95.83 ± 0.12	—	146.88 ± 0.25	61.56 ± 0.25	99.364 ± 0.080	—
Fit parameters						
P	10.2130447 ± 0.0000040	10.020195 ± 0.000020	$19.412378^{+0.000010}_{-0.000014}$	$25.208811^{+0.000015}_{-0.000018}$	$57.321927^{+0.000093}_{-0.000065}$	26.04626 ± 0.00035
e	$0.00183846^{+0.000043}_{-0.000046}$	0.0093 ± 0.00047	$0.194966^{+0.000050}_{-0.000054}$	$0.101283^{+0.000047}_{-0.000045}$	$0.305100^{+0.000034}_{-0.000031}$	$0.25051^{+0.00048}_{-0.00056}$
w	$4.730^{+0.024}_{-0.015}$	$6.188^{+0.042}_{-0.033}$	$4.94798^{+0.00045}_{-0.00042}$	$5.45092^{+0.00068}_{-0.00061}$	$6.23339^{+0.00011}_{-0.00018}$	$1.5652^{+0.0054}_{-0.0060}$
K	$48479.0^{+2.5}_{-2.2}$	10099.4 ± 4.5	$26488.66^{+0.97}_{-1.30}$	35116.0 ± 1.4	$28852.48^{+0.89}_{-0.99}$	$8169.5^{+4.7}_{-4.3}$
q	$0.623362^{+0.000083}_{-0.000065}$	$0.72090^{+0.00045}_{-0.00050}$	$0.86095^{+0.00017}_{-0.00013}$	$0.78692^{+0.00014}_{-0.00011}$	$0.786314^{+0.000119}_{-0.000098}$	$0.94962^{+0.00068}_{-0.00075}$
$\dot{\omega}$	0 ± 1000	0 ± 1000	158 ± 62	-60 ± 100	21^{+34}_{-27}	340 ± 700
T_{per}	$2459483.099^{+0.039}_{-0.024}$	$2459300.427^{+0.068}_{-0.051}$	2459409.0138 ± 0.0014	$2459374.6961^{+0.0026}_{-0.0023}$	$2459378.81855^{+0.00072}_{-0.00191}$	2459442.694 ± 0.022
$V_{\text{sys,pri}}$	-4800.8 ± 2.1	$-6558.4^{+3.9}_{-4.3}$	$9608.6^{+2.2}_{-2.0}$	-46047.8 ± 1.2	-5630.6 ± 1.0	6597.0 ± 4.5
$V_{\text{sys,sec}}$	-4240.2 ± 6.1	-6347.3 ± 6.2	$9961.6^{+4.1}_{-3.9}$	$-45670.7^{+6.0}_{-5.5}$	-5616.1 ± 4.0	$7659.2^{+5.1}_{-4.9}$
Derived parameters						
$M_{\text{pri}} \sin^3(i)$	1.31174 ± 0.00031	0.0084530 ± 0.0000095	0.191406 ± 0.000067	0.72977 ± 0.00026	0.80864 ± 0.00024	$0.0059273^{+0.0000098}_{-0.0000102}$
$M_{\text{sec}} \sin^3(i)$	0.81769 ± 0.00013	0.0060937 ± 0.0000060	$0.164793^{+0.000032}_{-0.000034}$	0.57427 ± 0.00011	0.63585 ± 0.00011	0.0056283 ± 0.0000077
M_{pri}	1.33233 ± 0.00092	—	1.173 ± 0.024	1.0733 ± 0.0076	$0.84184 \pm 6.4e-04$	—
M_{sec}	$0.83051 \pm 5.5e-04$	—	1.010 ± 0.021	0.8446 ± 0.0060	$0.66197 \pm 4.7e-04$	—
a_{bin}	$0.119137 \pm 2.7e-05$	—	0.1834 ± 0.0012	$0.20905 \pm 4.9e-04$	$0.333335 \pm 8.2e-05$	—
a_{pri}	0.045747 ± 0.000010	—	$0.08484^{+5.8e-04}_{-5.6e-04}$	$0.09206 \pm 2.2e-04$	$0.146733 \pm 3.4e-05$	—
a_{sec}	0.073390 ± 0.000018	—	$0.09854^{+6.7e-04}_{-6.5e-04}$	$0.11699 \pm 2.8e-04$	$0.186602 \pm 5.1e-05$	—
Bayes Factor $N_p = 1/N_p = 0$	1.6	6.6	2.1	0.4	1.2	40.6
mean $\sigma_{\text{RV,pri}}$	11.6	4.2	4.3	4.9	4.4	8.6
mean $\sigma_{\text{RV,sec}}$	44.3	29.0	14.8	29.1	9.3	9.5
rms_{pri}	12.5	18.1	6.2	5.8	4.8	10.6
rms_{sec}	40.3	24.9	21.0	63.4	27.3	20.6
Jitter _{pri}	< 4.0	14.9 ± 3.2	< 2.9	< 1.4	< 2.6	< 3.0
Jitter _{sec}	< 8.3	< 5.1	$12.3^{+5.1}_{-9.3}$	< 10.1	$25.6^{+3.4}_{-3.6}$	< 12.6

Note: Inclination values were obtained from previous literature sources: [Boden et al. \(2006\)](#) for HD 9939, [Konacki et al. \(2009\)](#) for HD78418 and HD 210027, and [Torres et al. \(2002\)](#) for HD195987. No inclination measurements were found for HD 13974 and HD 282975.

Standing M. R., et al., 2022, *MNRAS*, 511, 3571
 Standing M. R., et al., 2023, *Nature Astronomy*, 7, 702
 Sybilski P., Konacki M., Kozłowski S. K., Helminiak K. G., 2013, *Monthly Notices of the Royal Astronomical Society*, 431, 2024
 Torres G., Boden A. F., Latham D. W., Pan M., Stefanik R. P., 2002, *AJ*, 124, 1716
 Triaud A. H. M. J., et al., 2022, *Monthly Notices of the Royal Astronomical Society*, 511, 3561
 Trotta R., 2008, *Contemporary Physics*, 49, 71
 Zechmeister M., Kürster M., 2009, *A&A*, 496, 577
 Zucker S., Alexander T., 2007, *The Astrophysical Journal*, 654, L83
 Zucker S., Mazeh T., Santos N. C., Udry S., Mayor M., 2004, *A&A*, 426, 695

APPENDIX A: OBSERVED AND MODELLED RADIAL VELOCITIES

APPENDIX B: UNCERTAINTIES AND RMS VALUES

During our analysis, we attempted to compare the RMS values obtained from our *kima-DOLBY* analysis with those reported by (Konacki et al. 2009) for all our target systems. In Figure B1, the uncertainties are shown, where the box plot shows the distribution of uncertainties and the circles indicate the RMS for each binary system and compares them to other results. We focused on Keck/HIRES data for comparison, as this instrument provided the highest-precision measurements used by Konacki et al. (2009). For the case of HD 13974, as it was not observed with Keck/HIRES, we used the numbers from the Shane/CAT/Hamspec dataset (see Table 1 in Konacki et al. 2009), which was the only available data.

Upon re-analysing the (Konacki et al. 2010) RVs with *kima*, we found that RMS values were consistently higher than those reported. This discrepancy prevented a meaningful comparison between the results and also questioning accuracy of the RMS values.

Although this re-analysis was carried out for just HD 78418 and HD 210027 in detail, the consistent overestimation of RMS values suggests that similar discrepancies might exist for other systems as well.

APPENDIX C: DETECTION LIMITS

When comparing the detection limits of the Konacki data with *kima* (we call *kima-Konacki*) and with their own analysis (we call Konacki et al. 2009), we find that while they are comparable in terms of their overall significance, they exhibit different shapes. In Figure C1, we show the comparison of these detection limits for HD 78418 and HD 210027. Both sets of detection limits using Konacki et al. (2009) data are significantly above the detection limits obtained from our *kima-DOLBY* analysis, indicating that our *kima-DOLBY* method is more sensitive in detecting potential exoplanets.

In Figure C2, we scale the planet detection limits from Konacki et al. (2009) to number of observations and compare with DOLBY detection limits. Our method consistently performs better than previous approaches in detecting exoplanets. This improvement is due to both our DOLBY method's accuracy and the increased number of measurements. Even when accounting for the number of measurements, DOLBY still demonstrates significantly better detection limits. This suggests that DOLBY's underlying methodology is a key factor in our improved performance.

APPENDIX D: RADIAL VELOCITY DATA

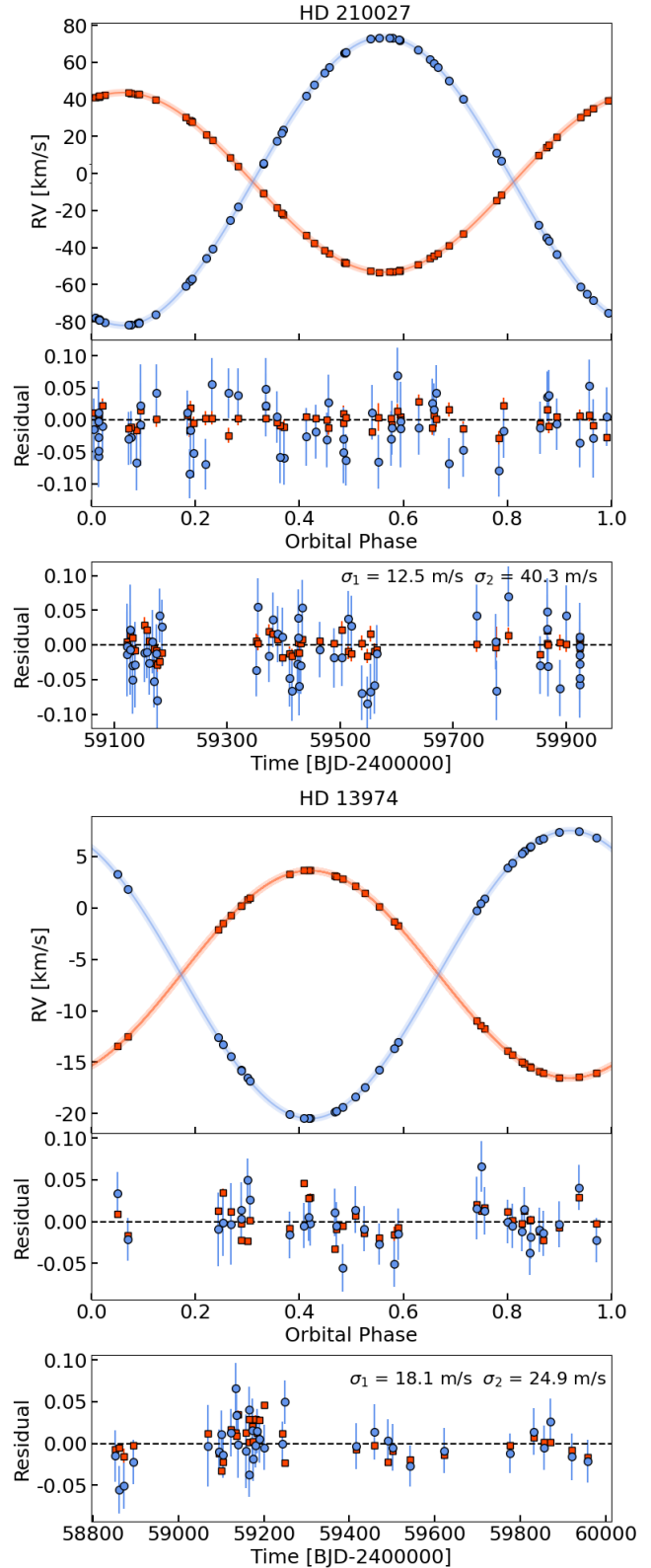


Figure A1. Observed and modelled radial velocities of HD 210027 and HD 13974 as a function of the orbital phase, their best-fit residuals as a function of the orbital phase and time. The orange squares and the blue circle symbols represent the primary and the secondary stars, respectively.

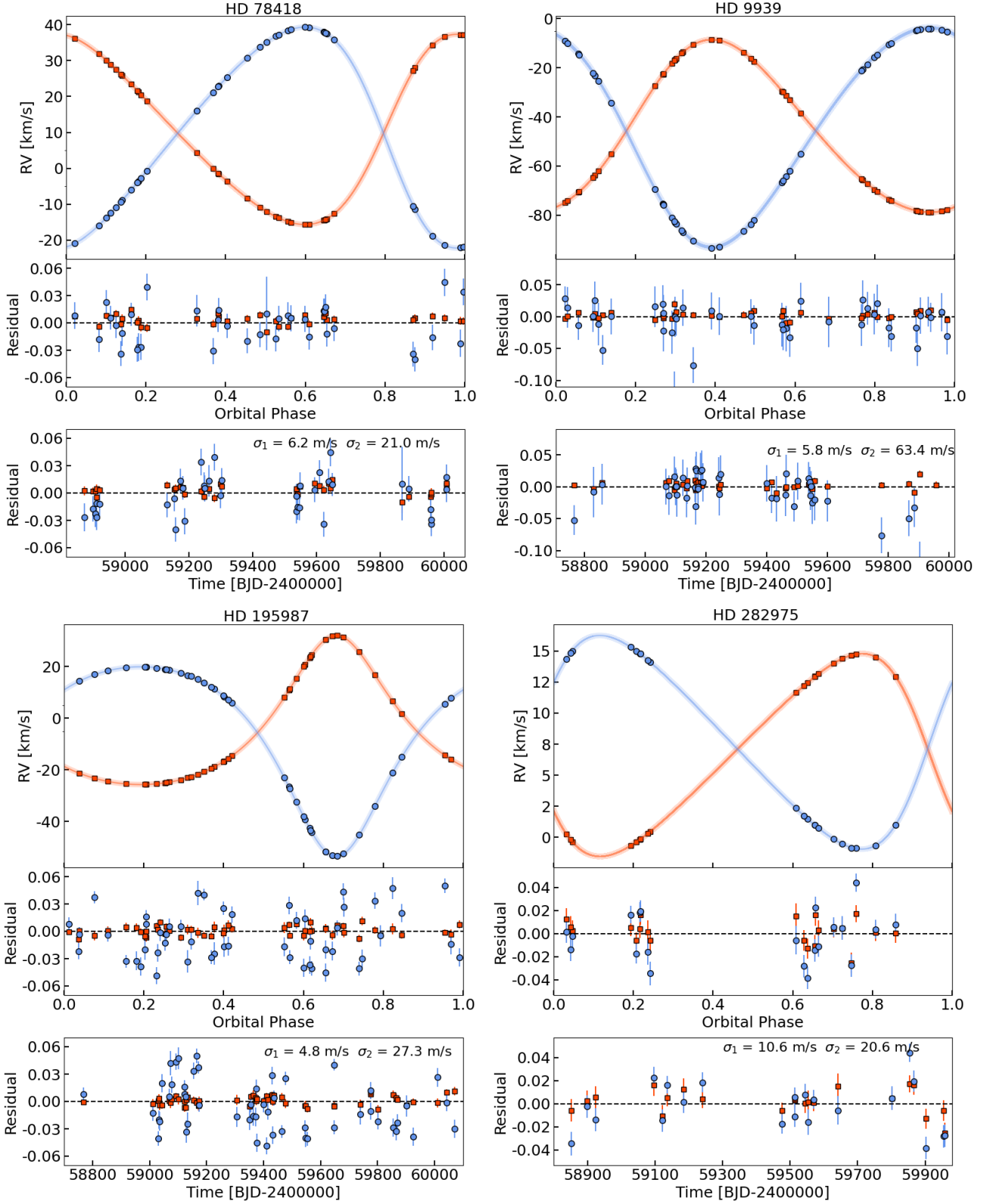


Figure A2. Observed and modelled radial velocities of HD 78418, HD 9939, HD 195987 and HD 282975 as a function of the orbital phase, their best-fit residuals as a function of the orbital phase and time. The orange squares and the blue circle symbols represent the primary and the secondary stars, respectively.

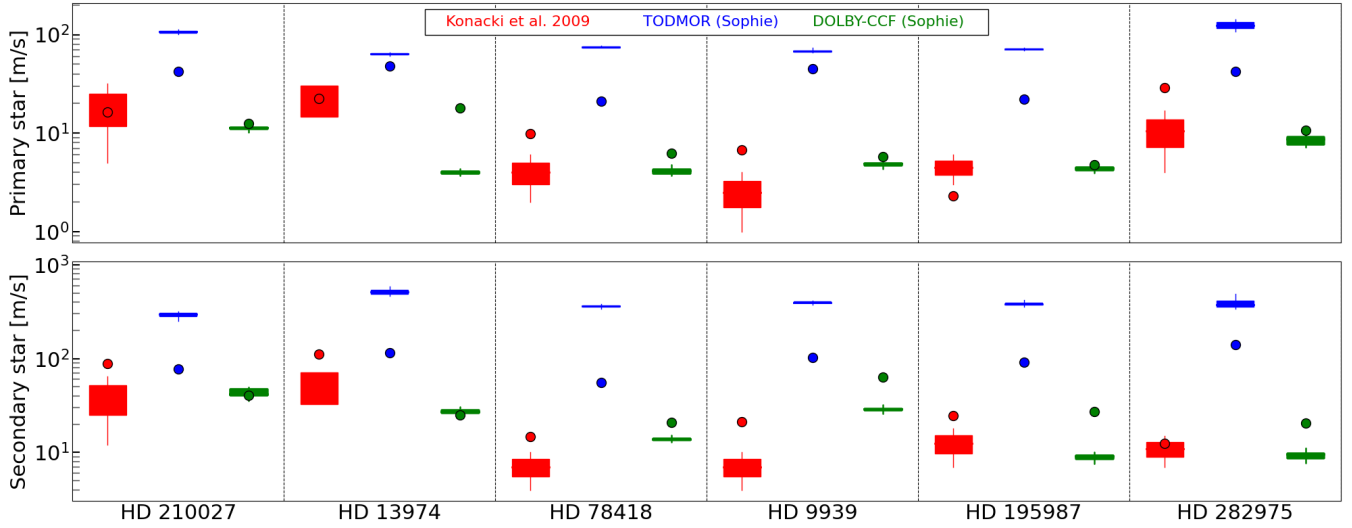


Figure B1. The uncertainties are presented for three measurement methods: Konacki et al. 2009 (Keck/HIRES) - shown in red, TODMOR (Sophie) - shown in blue, and DOLBY-CCF (Sophie) - shown in green. Box plots represent the distribution of uncertainties associated with each method for both primary (top panel) and secondary (bottom panel) stars. Additionally, RMS values for each method are plotted as scattered points with the corresponding colours. Note: For HD 13974, data from the Shane/CAT/Hamspec instrument (as reported in Konacki et al. 2009) were used, as Keck/HIRES observations were not available for this system.

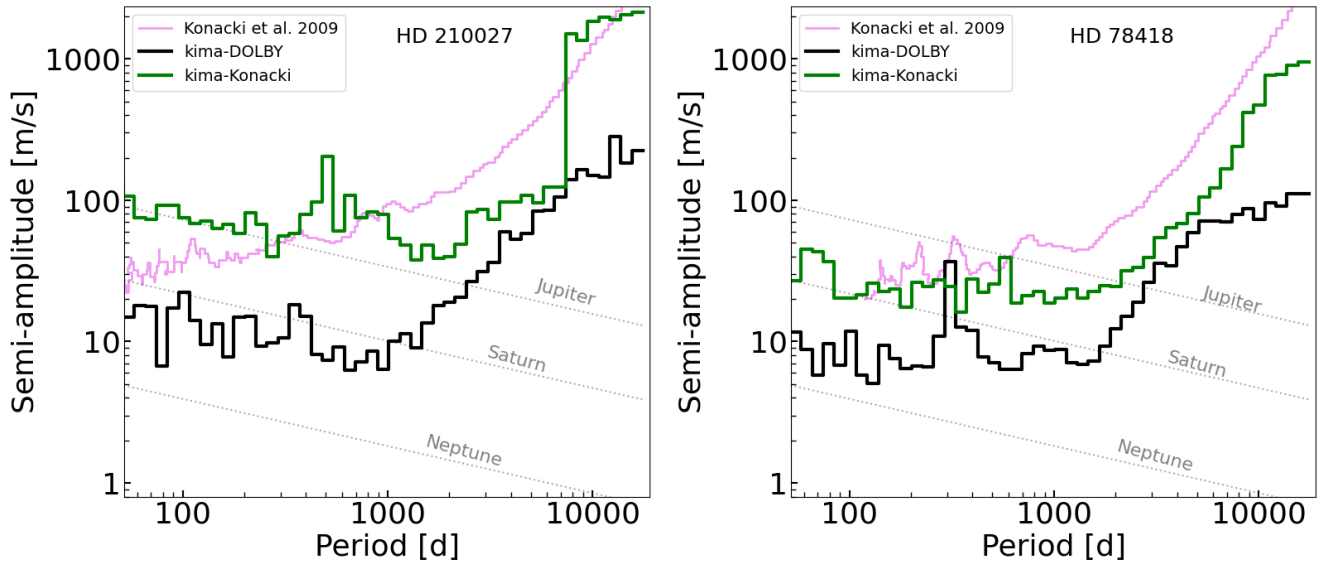


Figure C1. Detection limits based on the density of posterior samples for the HD 210027 and HD 78418 binary systems from the *kima* run with N_P fixed to 1. Solid lines represent the amplitude at the 99th percentile within each period bin, providing a 99% confidence upper limit. The black line indicates the combined dataset analysis, while the green line shows the analysis using the *kima*-Konacki derived data. The violet curve represents the planet detection limit from Konacki et al. (2009). Diagonal grey lines mark the expected signals for Neptune, Saturn, and Jupiter mass planets orbiting stars with their respective masses.

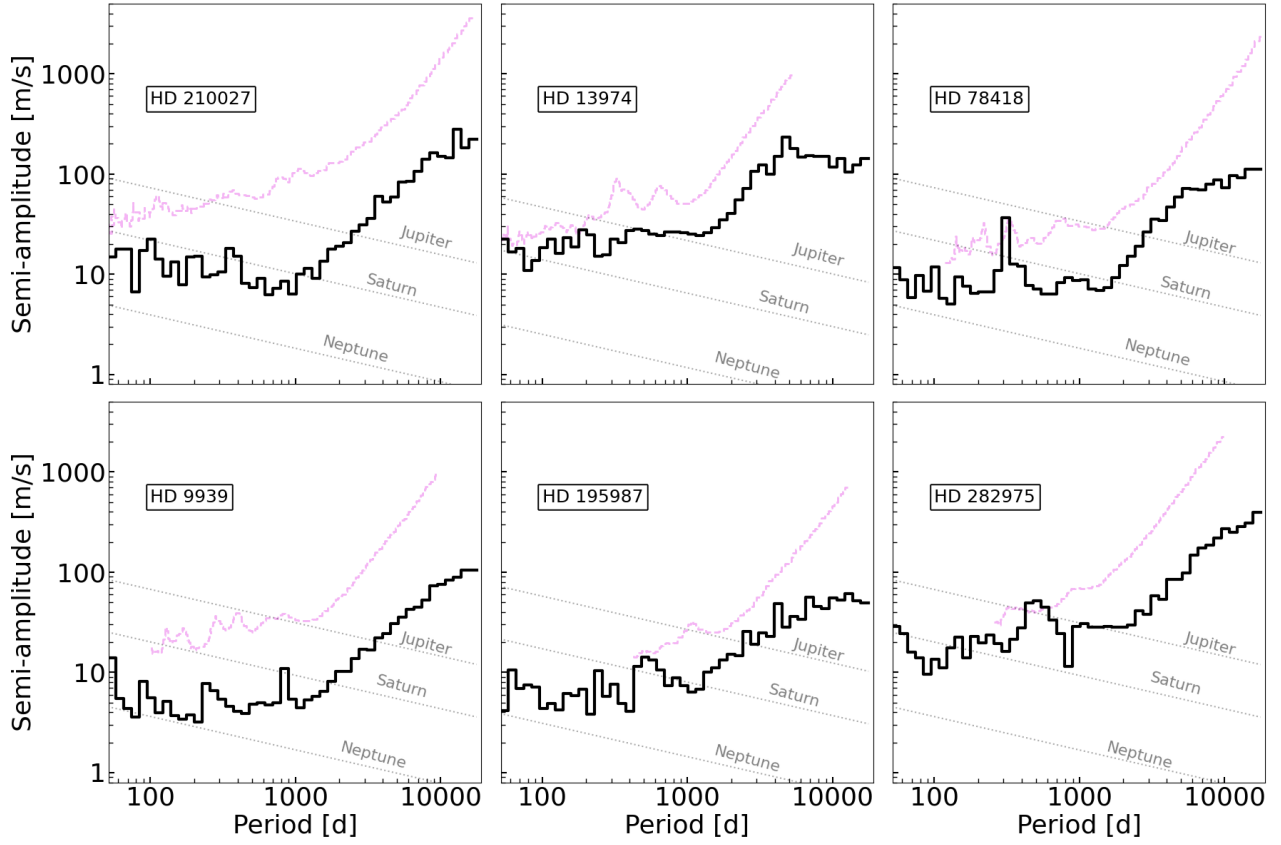


Figure C2. Detection limits for binary systems from the *kima* run with N_p fixed to 1. Histograms represent the distribution of semi-amplitudes within each period bin, with the vertical lines indicating the 99th percentile, corresponding to a 99% confidence upper limit. The violet curves show the planet detection limits from Konacki et al. (2009, 2010), scaled to the number of observations obtained for our paper, to enable as close to a like for like comparison as possible. The diagonal gray lines represent the expected signals of Neptune, Saturn, and Jupiter mass planets orbiting stars with their respective binary masses.

Table D1. RV Data for HD 210027 using Dolby CCF Method on Sophie Spectrum

BJD [days]	RV ₁ [km s ⁻¹]	σ_{RV_1} [km s ⁻¹]	O-C ₁ [km s ⁻¹]	RV ₂ [km s ⁻¹]	σ_{RV_2} [km s ⁻¹]	O-C ₂ [km s ⁻¹]
2459123.38091	-52.34232	0.01335	0.00938	72.11175	0.06193	-0.01038
2459123.38979	-52.29537	0.01307	0.00453	72.01824	0.06096	-0.02087
2459128.45234	42.93887	0.01271	0.01924	-80.69803	0.06467	0.01439
2459128.48099	42.75522	0.01251	-0.00456	-80.47051	0.06449	-0.01475
2459132.51401	-47.98416	0.01216	0.01493	65.10774	0.04950	-0.03731
2459132.51798	-48.05310	0.01206	-0.00057	65.17262	0.04864	-0.05809
2459137.39725	35.19619	0.01284	-0.00349	-68.35485	0.06139	-0.03636
2459154.37782	-49.12542	0.01119	0.03364	66.98514	0.04214	-0.01948
2459158.44617	42.58362	0.01174	0.02644	-80.14782	0.03846	-0.01739
2459162.39265	-33.48042	0.01064	0.01004	41.85057	0.04570	-0.03419
2459168.33550	39.52619	0.01138	-0.02196	-75.30244	0.04575	-0.00299
2459170.35326	28.16629	0.01078	-0.00049	-57.08909	0.03863	-0.05967
2459174.31727	-52.94527	0.01137	-0.00282	73.04889	0.04186	-0.02013
2459176.35188	-14.50687	0.01179	-0.02429	11.31581	0.04117	-0.08710
2459181.33461	8.41498	0.01145	-0.01973	-25.32817	0.03894	0.03443
2459185.26110	-45.73935	0.01163	-0.00722	61.52951	0.03888	0.01826
2459351.62279	30.55845	0.01095	0.01034	-60.89566	0.03765	-0.04413
2459354.61166	17.93299	0.01050	0.00754	-40.54485	0.04092	0.04753
2459374.58515	28.81861	0.01051	0.02387	-58.06133	0.03695	-0.02396
2459381.58875	14.16772	0.01027	0.02032	-34.50062	0.03904	0.02841
2459389.60043	-44.41779	0.01143	0.01247	59.43247	0.04067	0.00821
2459398.56787	-52.70122	0.01133	-0.01393	72.66380	0.04248	0.00383
2459410.59366	-32.47557	0.01028	-0.00835	40.18931	0.04127	-0.05512
2459414.44339	42.76507	0.01115	-0.01156	-80.55705	0.04341	-0.07423
2459424.49613	43.46540	0.01114	-0.00656	-81.63438	0.04170	-0.03518
2459425.57194	30.45091	0.01052	0.01262	-60.67250	0.03548	0.00302
2459426.60554	3.87457	0.01105	0.00766	-18.00283	0.04177	0.03073
2459427.49154	-22.03691	0.01100	-0.00689	23.44005	0.04240	-0.06716
2459429.57455	-53.12680	0.01122	0.00713	73.33900	0.04205	-0.03692
2459433.45656	33.09481	0.01060	0.01271	-64.87356	0.04046	0.04559
2459463.49870	19.65339	0.01058	0.01002	-43.36343	0.03972	-0.01442
2459489.37951	-37.38137	0.01114	0.00679	48.10777	0.04249	-0.02636
2459503.26544	-11.62182	0.01189	0.02698	6.83203	0.04118	-0.02556
2459514.40352	15.37954	0.01102	-0.00493	-36.48393	0.03982	0.03028
2459520.30192	-43.10972	0.01134	-0.00755	57.31461	0.04368	0.01968
2459538.32512	21.05451	0.01098	0.00717	-45.67957	0.03954	-0.07695
2459548.24825	27.88614	0.01079	-0.01125	-56.68909	0.03870	-0.09207
2459553.30195	-38.75507	0.01120	0.02067	50.28388	0.03966	-0.07523
2459560.22768	-21.10140	0.01147	-0.00414	21.94564	0.04147	-0.06566
2459565.27406	9.95154	0.01123	-0.00173	-27.81866	0.04056	-0.01984
2459741.57939	40.04336	0.01126	0.00540	-76.05172	0.04490	0.03423
2459774.60436	-18.34614	0.01109	0.00123	17.59785	0.04022	-0.00323
2459776.61296	-53.18037	0.02209	0.00901	73.39141	0.04257	-0.07335
2459797.43653	-52.36365	0.01130	0.01846	72.23316	0.04337	0.06229
2459853.40173	43.56933	0.01094	-0.00846	-81.80592	0.04184	-0.03683
2459866.25707	-10.62429	0.01320	0.02584	5.27034	0.04887	0.01512
2459866.26082	-10.75328	0.01319	0.00745	5.47359	0.04757	0.04095
2459867.45408	-41.37190	0.01131	0.00510	54.49047	0.04287	-0.03873
2459888.30601	-48.34365	0.01142	0.00867	65.64090	0.04064	-0.07038
2459900.31845	-43.26153	0.01145	0.00560	57.59416	0.04333	0.03451
2459924.23470	41.02977	0.01158	0.01571	-77.67567	0.04813	-0.02275
2459924.30571	41.67963	0.01133	0.01377	-78.76368	0.04836	-0.06429
2459924.30953	41.70923	0.01134	0.01082	-78.76205	0.04827	-0.01040
2459924.31335	41.73751	0.01140	0.00679	-78.83872	0.04868	-0.03522
2459924.31714	41.76263	0.01127	0.00013	-78.85060	0.04891	0.00394
2459924.32097	41.80818	0.01133	0.01381	-78.96153	0.04902	-0.05582

Table D2. RV Data for HD 13974 using Dolby CCF Method on Sophie Spectrum

BJD [days]	RV ₁ [km s ⁻¹]	σ_{RV_1} [km s ⁻¹]	O-C ₁ [km s ⁻¹]	RV ₂ [km s ⁻¹]	σ_{RV_2} [km s ⁻¹]	O-C ₂ [km s ⁻¹]
2458851.36986	-1.73619	0.00467	-0.00665	-13.04684	0.03064	-0.01498
2458860.32662	2.80378	0.00399	-0.00540	-19.38319	0.02867	-0.05570
2458871.33474	-1.32472	0.00887	-0.01535	-13.66542	0.02769	-0.05077
2458895.26721	-16.07826	0.00392	-0.00223	6.84277	0.02696	-0.02227
2459068.59190	-0.72497	0.00391	0.01157	-14.41216	0.04891	-0.00296
2459094.56982	-15.89868	0.00386	-0.01229	6.59235	0.02681	-0.00972
2459100.65292	3.13285	0.00405	-0.03291	-19.81134	0.02858	0.01077
2459104.66467	-16.06569	0.00388	-0.02251	6.80556	0.02724	-0.01393
2459123.57672	-11.74338	0.00401	0.01705	0.89295	0.02872	0.01266
2459133.53153	-11.39425	0.00434	0.01315	0.45675	0.03071	0.06606
2459136.54978	-13.45844	0.00373	0.00943	3.28183	0.02582	0.03366
2459138.58370	-1.51518	0.00431	0.03473	-13.28270	0.03927	-0.00169
2459158.53279	-2.05556	0.00539	0.01251	-12.57175	0.04432	-0.00944
2459164.52865	-15.41809	0.00382	0.00156	5.91695	0.02634	-0.03787
2459165.48529	-16.47060	0.00399	0.02934	7.49353	0.02685	0.04064
2459173.53048	-10.93347	0.00542	0.02043	-0.22219	0.03723	0.01605
2459174.57244	-15.48454	0.00384	0.00199	6.02874	0.02634	-0.01881
2459180.33942	3.66827	0.00408	0.02940	-20.48049	0.02669	-0.00209
2459184.46913	-15.10267	0.00382	0.01293	5.54808	0.02630	0.01491
2459190.33616	3.66605	0.00410	0.02769	-20.47263	0.02809	0.00505
2459200.25548	3.65633	0.00411	0.04599	-20.44373	0.02720	-0.00491
2459244.27223	-13.92165	0.00373	0.01211	3.89420	0.02600	-0.00005
2459249.27867	0.81736	0.00393	-0.02331	-16.54747	0.02595	0.04944
2459415.60524	-16.48543	0.00400	-0.00738	7.41897	0.02737	-0.00356
2459459.57600	0.25367	0.00506	-0.00209	-15.77196	0.03292	0.01363
2459489.63908	0.24514	0.00387	-0.02267	-15.79874	0.02523	0.00356
2459501.49659	3.08327	0.00404	-0.00942	-19.72562	0.02812	-0.00485
2459542.39883	0.16392	0.00384	-0.01913	-15.71181	0.02459	-0.02705
2459622.27606	1.42672	0.00393	-0.01359	-17.43741	0.02701	-0.00872
2459775.60673	-14.94069	0.00399	-0.00263	5.27494	0.02393	-0.01203
2459832.51807	2.12060	0.00397	0.00688	-18.34861	0.02794	0.01418
2459855.59138	-14.28766	0.00379	0.00169	4.38260	0.02654	-0.00477
2459870.56860	1.00991	0.00412	0.00156	-16.80347	0.02777	0.02604
2459921.44118	3.32644	0.00407	-0.00759	-20.07147	0.02768	-0.01594
2459958.40976	-12.50915	0.00371	-0.01640	1.87455	0.02592	-0.02132

Table D3. RV Data for HD 78418 using Dolby CCF Method on Sophie Spectrum

BJD [days]	RV ₁ [km s ⁻¹]	σ_{RV_1} [km s ⁻¹]	O-C ₁ [km s ⁻¹]	RV ₂ [km s ⁻¹]	σ_{RV_2} [km s ⁻¹]	O-C ₂ [km s ⁻¹]
2458872.37870	21.27676	0.00478	0.00243	-3.59807	0.01528	-0.02680
2458898.49292	-13.47233	0.00378	0.00228	36.76581	0.01414	-0.01753
2458907.47357	37.24499	0.00416	0.00233	-22.09402	0.01499	-0.02255
2458910.41886	25.84510	0.00446	0.00470	-8.88600	0.01388	-0.01146
2458911.33579	20.48118	0.00424	-0.00490	-2.68233	0.01424	-0.02657
2458920.37977	-14.04810	0.00372	0.00328	37.47144	0.01403	-0.01192
2459130.66567	-10.87384	0.00391	0.00873	33.76031	0.01343	-0.01297
2459153.68550	-12.63554	0.00369	0.00408	35.81088	0.01367	-0.00611
2459157.62496	28.01406	0.00432	0.00501	-11.42754	0.01325	-0.04023
2459172.58339	-14.51336	0.00372	0.00670	38.01254	0.01380	0.01307
2459181.62800	28.94156	0.00416	0.00581	-12.46418	0.01292	0.00555
2459186.60880	-0.01687	0.00412	-0.00104	21.14648	0.01415	-0.03093
2459237.62907	37.11821	0.00416	0.00216	-21.93676	0.01489	0.03397
2459248.49694	-14.84864	0.00402	-0.00381	38.38285	0.01461	0.00819
2459248.63740	-15.08212	0.00381	0.00540	38.66170	0.01424	0.00514
2459263.45847	4.40171	0.00510	0.00464	16.01318	0.01736	0.01311
2459280.45118	18.80057	0.00418	-0.00563	-0.66523	0.01464	0.03949
2459298.35123	27.60645	0.00439	0.00968	-10.91746	0.01347	-0.00294
2459303.36350	-1.53055	0.00416	0.00713	22.93540	0.01345	0.01393
2459536.71790	-3.63984	0.00433	0.00221	25.31719	0.01362	-0.00330
2459537.69503	-8.28468	0.00422	0.00437	30.72184	0.01352	-0.01972
2459540.71828	-15.61997	0.00388	-0.00113	39.25905	0.01431	-0.01525
2459546.72643	34.37384	0.00399	0.00767	-18.79004	0.01386	-0.01617
2459548.72050	36.20188	0.00411	0.00708	-20.89273	0.01468	0.00826
2459594.52691	-1.41021	0.00420	0.01081	22.78949	0.01379	0.00348
2459608.48351	30.07109	0.00402	0.00787	-13.75660	0.01311	0.02268
2459623.43923	27.20333	0.00442	0.00343	-10.48153	0.01340	-0.03430
2459638.50612	-14.43425	0.00382	0.01078	37.92500	0.01414	0.01261
2459644.38323	36.64494	0.00421	0.00544	-21.37130	0.01505	0.04458
2459648.51053	23.43053	0.00443	0.01470	-6.04911	0.01292	0.00938
2459868.64759	-12.01896	0.01200	-0.01003	35.03915	0.04037	0.01023
2459888.64574	-13.80355	0.00371	-0.00410	37.16529	0.01406	0.00471
2459957.53755	31.86693	0.00397	-0.00411	-15.93369	0.01387	-0.01783
2459958.61724	26.23676	0.00441	-0.00113	-9.37006	0.01354	-0.03385
2459959.41779	21.59474	0.00434	0.00075	-3.97159	0.01377	-0.02906
2460006.40723	-15.65450	0.00392	0.00856	39.29607	0.01421	0.00431
2460007.41061	-14.22850	0.00376	0.01059	37.69088	0.01387	0.01750

Table D4. RV Data for HD 9939 using Dolby CCF Method on Sophie Spectrum

BJD [days]	RV ₁ [km s ⁻¹]	σ_{RV_1} [km s ⁻¹]	O-C ₁ [km s ⁻¹]	RV ₂ [km s ⁻¹]	σ_{RV_2} [km s ⁻¹]	O-C ₂ [km s ⁻¹]
2458858.37230	-69.59819	0.00515	0.00270	-15.63101	0.03004	-0.05248
2459068.58880	-55.01951	0.00495	-0.00328	-34.21645	0.02903	-0.00851
2459077.63446	-17.38670	0.00501	0.00615	-82.06566	0.03015	0.00370
2459096.55610	-27.41804	0.00492	0.00596	-69.30955	0.02952	0.00033
2459100.64992	-8.86494	0.00498	0.00891	-92.88379	0.02824	-0.01363
2459102.62882	-16.15512	0.00490	-0.00481	-83.63979	0.02759	0.01531
2459104.61855	-29.54584	0.00513	-0.00086	-66.60837	0.03219	0.00029
2459123.55891	-13.54038	0.00483	0.00498	-86.98169	0.02947	0.00025
2459136.58872	-73.58189	0.00507	0.00056	-10.64629	0.03260	-0.01308
2459138.58018	-78.44756	0.00496	0.00302	-4.48104	0.03072	0.01384
2459164.41903	-78.74896	0.00489	-0.00195	-4.10826	0.03023	-0.01774
2459165.48006	-77.71594	0.00511	0.00895	-5.40001	0.03057	0.00166
2459166.49085	-74.77060	0.00505	0.00970	-9.13958	0.03140	-0.00145
2459168.38319	-63.83368	0.00511	-0.00559	-23.05031	0.03003	-0.03120
2459173.47593	-16.64036	0.00493	-0.00323	-83.01520	0.02886	0.02846
2459173.52642	-16.29119	0.00499	0.00384	-83.46716	0.02892	0.02492
2459181.43455	-38.62125	0.00508	0.00235	-55.08504	0.02845	-0.00032
2459185.33203	-65.65455	0.00515	0.00756	-20.73494	0.03146	-0.00352
2459190.32281	-78.30099	0.00493	0.00660	-4.67014	0.03023	0.02450
2459242.29567	-74.04520	0.00514	0.00174	-10.09967	0.03274	0.02638
2459244.24760	-61.97739	0.00524	0.00606	-25.41548	0.03208	0.00685
2459248.33469	-22.62320	0.00504	0.00028	-75.38557	0.03036	0.01407
2459399.59509	-22.57071	0.00497	-0.00231	-75.47639	0.02970	-0.01187
2459415.60256	-78.12005	0.00502	0.00291	-4.88995	0.03065	0.01973
2459432.57414	-31.36037	0.00599	-0.00282	-64.31752	0.03795	0.00535
2459462.56743	-65.31155	0.00512	0.00724	-21.18090	0.03105	-0.01767
2459463.56289	-70.45211	0.00518	-0.01031	-14.63985	0.02922	-0.01885
2459489.64627	-74.07999	0.00512	-0.00204	-10.02058	0.03289	-0.01304
2459503.46598	-8.53155	0.00502	-0.00012	-93.33199	0.02811	0.02007
2459538.55434	-67.29364	0.00513	-0.00023	-18.64480	0.03261	-0.03109
2459542.39462	-78.74315	0.00494	0.00154	-4.10112	0.03110	0.00871
2459545.46940	-70.75187	0.00515	0.00295	-14.24031	0.02945	0.01263
2459546.41498	-64.59449	0.00514	0.00243	-22.06312	0.03049	0.00750
2459551.40013	-18.13658	0.00515	0.00577	-81.10746	0.03288	-0.01380
2459558.43304	-29.96531	0.00520	-0.00159	-66.06794	0.03387	0.00023
2459601.29306	-22.33338	0.00497	-0.00309	-75.75891	0.02978	-0.02485
2459779.61956	-10.65818	0.00492	0.00909	-90.54018	0.03178	-0.02012
2459797.62825	-70.34967	0.00519	0.00081	-14.64547	0.03007	-0.02225
2459854.52788	-14.02566	0.00486	0.00269	-86.19184	0.02820	-0.07637
2459869.42980	-78.21860	0.00496	0.00456	-4.61381	0.03050	-0.04957
2459886.56099	-33.09126	0.00509	-0.00906	-61.95479	0.02905	-0.03289
2459904.48732	-16.94018	0.00501	0.01999	-82.44737	0.02987	-0.11632
2459959.27294	-13.77033	0.00482	0.00285	-86.42047	0.02921	0.29986

Table D5. RV Data for HD 195987 using Dolby CCF Method on Sophie Spectrum

BJD [days]	RV ₁ [km s ⁻¹]	σ_{RV_1} [km s ⁻¹]	O-C ₁ [km s ⁻¹]	RV ₂ [km s ⁻¹]	σ_{RV_2} [km s ⁻¹]	O-C ₂ [km s ⁻¹]
2458767.44980	-19.58729	0.00347	-0.00068	12.15788	0.00770	0.00767
2459010.57241	-24.99781	0.00519	-0.00263	19.01268	0.00888	-0.01264
2459031.58433	24.52511	0.00415	0.00087	-43.97312	0.00784	-0.04054
2459033.60485	30.51372	0.00442	0.00342	-51.56721	0.01024	-0.01998
2459034.55544	31.80618	0.00506	-0.00414	-53.22300	0.01027	-0.02187
2459044.54125	1.75428	0.00399	-0.00375	-14.96329	0.01010	0.02017
2459068.48549	-24.73894	0.00355	0.00059	18.70550	0.00891	0.00512
2459072.53538	-21.77383	0.00582	-0.00152	14.97086	0.01324	0.04196
2459077.47004	-14.56690	0.00376	0.00261	5.79191	0.00899	0.01842
2459093.48616	31.30272	0.00377	0.00578	-52.50469	0.00909	0.04346
2459100.50645	6.67546	0.00598	0.00272	-21.18494	0.01203	0.04708
2459122.46379	-25.65979	0.00465	-0.00675	19.86971	0.00706	0.00826
2459122.48541	-25.65150	0.00417	-0.00033	19.87494	0.00747	0.01586
2459127.40713	-23.83828	0.00342	-0.00694	17.55151	0.00698	0.00547
2459128.44366	-23.06215	0.00526	0.00214	16.53802	0.01249	-0.03307
2459132.26642	-18.82948	0.00611	0.00454	11.16976	0.01254	-0.02435
2459155.30948	16.79037	0.00418	0.00138	-34.06186	0.00883	0.03363
2459165.33216	-14.33204	0.00283	-0.00104	5.51959	0.00822	0.04999
2459172.35297	-23.24635	0.00510	-0.00492	16.83323	0.00677	0.03730
2459174.27477	-24.46398	0.00422	0.00084	18.34732	0.00755	-0.00367
2459305.64369	-16.61477	0.00566	0.00146	8.35839	0.01098	-0.01670
2459351.61913	-25.66858	0.00439	-0.00534	19.85431	0.01154	-0.02010
2459354.60816	-24.94729	0.00360	0.00534	18.96805	0.00897	-0.00318
2459363.54500	-15.57905	0.00500	0.00688	7.04920	0.01023	-0.01627
2459371.59079	8.05734	0.00568	0.00399	-23.00347	0.01043	-0.01700
2459374.60037	20.87997	0.00439	0.00052	-39.28299	0.01012	0.01382
2459377.52102	30.48196	0.00470	0.00299	-51.55269	0.00998	-0.04533
2459399.44040	-21.26427	0.00414	0.00068	14.28020	0.00838	-0.00339
2459410.58249	-25.39247	0.00386	0.00577	19.48908	0.00917	-0.04853
2459415.50033	-22.68478	0.00408	0.00184	16.07992	0.00904	-0.01112
2459429.57920	10.84287	0.00366	0.00714	-26.49598	0.00956	0.02835
2459432.56152	23.46212	0.00445	-0.00028	-42.61899	0.00980	-0.03699
2459436.49438	32.01894	0.00414	0.00667	-53.45443	0.00861	0.00369
2459463.48393	-25.43569	0.00453	0.00459	19.55807	0.00679	-0.03288
2459477.48547	-16.82898	0.00492	-0.00224	8.66785	0.00728	0.02519
2459544.32381	11.25872	0.00382	-0.00440	-27.09618	0.00771	-0.02841
2459546.35246	19.97966	0.00529	-0.00447	-38.19812	0.01023	-0.04000
2459554.28903	25.65379	0.00382	-0.00800	-45.42088	0.00755	-0.04084
2459646.69694	-20.74314	0.00373	-0.00458	13.65525	0.00663	0.04032
2459647.70492	-19.47515	0.00380	-0.00519	11.97384	0.00762	-0.02860
2459739.49580	-16.01978	0.00545	-0.00318	7.59803	0.01082	-0.01423
2459774.57537	15.41881	0.00458	0.00781	-32.33024	0.00907	0.01204
2459776.61934	23.95970	0.00447	0.00989	-43.21266	0.00908	-0.01070
2459800.63752	-21.21510	0.00434	-0.00839	14.18785	0.00926	-0.02171
2459855.36671	-17.94399	0.00422	0.00763	10.04320	0.01014	-0.02873
2459866.26356	-25.66229	0.00430	0.00409	19.84599	0.01060	-0.03239
2459869.34471	-25.34610	0.00370	0.00232	19.45066	0.00956	-0.02363
2459901.24851	13.68083	0.00463	-0.00370	-30.15247	0.01161	-0.00477
2459924.21804	-25.68638	0.00385	-0.00038	19.86468	0.01016	-0.03864
2460010.70041	31.20871	0.00500	-0.00157	-52.41145	0.01030	0.02645
2460041.66411	-25.23418	0.00358	0.00975	19.34025	0.00947	-0.00124
2460070.62334	24.11113	0.00473	0.01144	-43.42312	0.00977	-0.02995

Table D6. RV Data for HD 282975 using Dolby CCF Method on Sophie Spectrum

BJD [days]	RV ₁ [km s ⁻¹]	σ_{RV_1} [km s ⁻¹]	O-C ₁ [km s ⁻¹]	RV ₂ [km s ⁻¹]	σ_{RV_2} [km s ⁻¹]	O-C ₂ [km s ⁻¹]
2458851.38469	0.45294	0.00978	-0.00576	14.09135	0.01029	-0.03460
2458898.38654	-0.37863	0.00897	0.00240	15.00823	0.00983	-0.00228
2458924.31871	-0.20532	0.00965	0.00559	14.81763	0.01026	-0.01379
2459096.59172	12.95871	0.00923	0.01624	1.00437	0.00954	0.02252
2459122.61784	12.91231	0.00945	-0.01052	0.98820	0.00975	-0.01433
2459136.62423	-0.67026	0.00729	0.00498	15.33625	0.00768	0.01638
2459184.50882	0.26131	0.00932	0.01278	14.34905	0.00934	0.00129
2459241.40466	-0.17399	0.00768	0.00414	14.81492	0.00863	0.01846
2459475.58271	-0.39070	0.00717	-0.00602	14.99645	0.00822	-0.01749
2459513.54933	13.15543	0.00809	0.00320	0.74992	0.00929	-0.01107
2459514.55909	14.01542	0.00750	0.00432	-0.13764	0.00858	0.00567
2459544.64636	12.94248	0.00833	0.00038	0.99053	0.00936	0.00777
2459554.47041	0.30082	0.00970	0.00159	14.27782	0.01111	-0.01603
2459569.38751	14.52205	0.00735	0.00098	-0.67618	0.00821	0.00387
2459642.30919	11.64299	0.01070	0.01542	2.36058	0.01226	-0.00574
2459801.61970	14.38294	0.00916	0.00460	-0.52525	0.01032	0.00472
2459854.62748	14.76487	0.00732	0.01723	-0.87450	0.00808	0.04427
2459866.54498	-0.13297	0.00848	0.01645	14.78591	0.00906	0.01968
2459903.52873	12.42914	0.00872	-0.01281	1.47036	0.00980	-0.03849
2459955.38046	12.18273	0.00876	-0.00584	1.74739	0.00981	-0.02825
2459958.48351	14.63086	0.00886	-0.02523	-0.84999	0.00968	-0.02759